Sensors and Actuators B 257 (2018) 347–353

Contents lists available at ScienceDirect

Sensors and Actuators B: Chemical

journal homepage: www.elsevier.com/locate/snb

Research Paper

Development of a semigraphitic sulfur-doped ordered mesoporous carbon material for electroanalytical applications

Jaqueline R. Maluta [a], Sergio A.S. Machado [a], Umesh Chaudhary [b], J. Sebastián Manzano [b], Lauro T. Kubota [c], Igor I. Slowing [b,*]

[a] São Carlos Institute of Chemistry, University of São Paulo, CP 380, CEP 13566-590, São Carlos, São Paulo, Brazil
[b] US DOE Ames Laboratory and Department of Chemistry, Iowa State University, Ames, IA 50011, United States
[c] Department of Analytical Chemistry, Institute of Chemistry – UNICAMP, P.O. Box 6154, 13084-971, Campinas, São Paulo, Brazil

ARTICLE INFO

Article history:
Received 28 June 2017
Received in revised form 13 October 2017
Accepted 27 October 2017
Available online 29 October 2017

Keywords:
Ordered mesoporous carbon
Sulfur-doped carbon
Mesoporous silica nanoparticles
Electrochemical sensor
Chloramphenicol detection

ABSTRACT

The modification of traditional electrodes with mesoporous carbons is a promising strategy to produce high performance electrodes for electrochemical sensing. The high surface area of mesoporous carbons provides a large number of electroactive sites for binding analytes. Controlling the pore size and structure of mesoporous carbons and modifying their electronic properties via doping offers additional benefits like maximizing transport and tuning the electrochemical processes associated with analyte detection. This work reports a facile method to produce sulfur-doped ordered mesoporous carbon materials (S-OMC) with uniform pore structure, large pore volume, high surface area and semigraphitic structure. The synthesis used thiophenol as a single source of carbon and sulfur, and iron as a catalyst for low temperature carbonization. The S-OMC material was deposited on a glassy carbon electrode and used as a sensor with high sensitivity (11.7 A L mol^{-1}) and selectivity for chloramphenicol detection in presence of other antibiotics. As a proof-of-concept, the sensor was applied to the direct analysis of the drug in reconstituted powdered milk and in commercial eye drops.

1. Introduction

Several different carbon materials are used in electroanalysis due to their electrical conductivity, chemical inertness, and low background current [1]. Nanostructured carbons such as ordered mesoporous carbons (OMC) have the additional benefits of uniform pore structures, large pore volumes, high specific surface areas, and tunable pore size distributions, which can maximize the interaction with analytes and ensure fast mass transport [2,3]. Furthermore, due to their fast electron transfer capacity and excellent electrocatalytic activity, OMC have been recently used in sensing [4], with excellent performance in detection of morphine, epinephrine, acetaminophen, H_2O_2, nitrobenzene, and NADH [5–7]. The superb electrochemical behavior of OMC may be attributed to a large number of edge plane defect sites on their accessible surface [6].

OMC are typically synthesized by infiltrating the pores of a mesoporous silica template with an appropriate carbon precursor, followed by carbonization, and subsequent silica removal [8]. The graphitic character of OMC determines their electrical conductivity, and is a key for their electrochemical applications [9]. A high graphitic character and electrical conductivity can be achieved by using aromatic precursors [10], carbonizing at high pressures [11], using chemical vapor deposition [12], or adding iron as carbonization catalyst [13,14].

The electronic properties of OMC can be controlled by incorporating heteroatoms into their structure. While nitrogen-doping of OMC has been widely explored [15], sulfur-doping is less common. S-doped OMC (S-OMC) have been obtained by post-synthesis treatment using melt-diffusion [16–18], or directly using sulfur-containing molecules like *p*-toluenesulfonic acid or benzyl disulfide as a source [19–21]. These S-doped materials have been used to promote metal-support interactions in the catalytic oxygen reduction reaction [21,24,25], and in the adsorption of acetaminophen [22,23], and dibenzothiophene [26,27].

Chloramphenicol (CAP) is a broad-spectrum antimicrobial with remarkable antibacterial and pharmacokinetic properties. However, this drug is considered an environmental contaminant and is forbidden for use in food-producing animals [28,29] because it is associated with human health issues such as aplastic anemia, hepatic dysfunction, gray syndrome, and cancer [30,31]. In spite of this status, the Rapid Alert System for Food and Feed (RASFF) of the European Union has reported over 500 notifications of the illegal

* Corresponding author.
E-mail address: islowing@iastate.edu (I.I. Slowing).

https://doi.org/10.1016/j.snb.2017.10.164
0925-4005/

use of CAP between 2004 and 2017 [32]. Therefore, detecting this drug has financial, environmental, and public health importance.

Herein, we report the synthesis and characterization of S-OMC with semi-graphitic character. The materials were prepared using thiophenol as an aromatic S-containing carbon precursor and iron as a catalyst. Because of their adsorptive and electrochemical properties, the materials were used to assemble modified electrodes for the direct detection and quantification of ppm levels of CAP.

2. Materials and methods

2.1. Preparation of S-OMC

SBA-15 type mesoporous silica nanoparticles (MSN) were synthesized following previous reports [33]. Briefly, 7.0 g of Pluronic P-104 surfactant were dissolved in 164 mL of Millipore water and 109 mL of HCl 4.0 mol L^{-1}. The solution was stirred for 1 h at 52 °C. Then, 10.6 g of tetramethyl orthosilicate (TMOS) were added and the solution was stirred for further 24 h at 52 °C. After this, the solution was placed in an autoclave for hydrothermal treatment at 150 °C for additional 24 h. The MSN product was then filtered, washed with ethanol and dried in air. The surfactant was removed by calcination in air at 550 °C for 6 h. Following a literature procedure [3,10], a solution of $Fe(NO_3)_3{\cdot}9H_2O$ in acetone (1.0 mL) was impregnated into the MSN (1.00 g), and calcined in air at 350 °C for 6 h. Three different concentrations of iron precursor (0.382, 0.764, or 1.145 g per mL of acetone) were used to evaluate the effect of the amount of iron on the synthesis of the carbon materials. Finally, the ordered mesoporous carbon (OMC) materials were synthesized by impregnating 1.00 g of the Fe-MSN composites with thiophenol (950 μL, 8.97 mmol), drying at 70 °C and carbonizing at 600 °C or 900 °C during 7 h under flowing Ar. The MSN template was removed by refluxing in a water:ethanol (1:1) solution of NaOH (1 mol L^{-1}) overnight at 80 °C (twice). The resulting S-OMC material was filtered out, washed with Millipore water and dried in air at 70 °C.

2.2. Characterization

Wide and low angle X-ray diffraction (XRD) patterns of the materials were acquired using a Shimadzu XRR7000 and a BRUKER APEX II Duo, respectively. Both diffractometers used Cu Kα (λ = 1.5405 Å) radiation source operating at 40 kV and 30 mA. Raman spectra of the materials were acquired on a confocal Horiba Scientific T64000 Raman spectrometer using a 633 nm laser as the excitation source. The surface area and porosity of the materials were measured by nitrogen sorption isotherms at 196 °C in a Micromeritics TriStar instrument after a 6 h pre-treatment at 100 °C under N_2 flow. The surface area and pore size distribution of the materials were calculated by the Brunauer–Emmett–Teller (BET) and the Barret–Joyner–Halenda (BJH) methods, respectively. Scanning electron microscopy (SEM) of the materials was performed with a JEOL JSM634 F equipped with Field Emission Gun (FEG). Energy dispersive spectra (EDS) of the materials were acquired using a ZEISS LEO 440 electron microscope (Cambridge, England) linked with an EDX LINK ANALYTICAL (Isis System Series 300) detector. Transmission electron microscopy (TEM) of the materials was performed in a LIBRA120 microscope.

2.3. Electrochemical measurements

The electrochemical measurements were performed in an AUTOLAB PGSTAT 12 system interfaced with NOVA software, using a three-electrode cell. Ag/AgCl (3 M KCl) and Pt foil (1.0 cm^2) were used as reference and counter electrodes respectively. The working electrode was prepared using a glassy carbon (GC) electrode (3 mm diameter). The GC electrode was polished with alumina and rinsed thoroughly with doubly distilled water. Then, 10.0 μL of the respective S-OMC dispersion (2.0 ± 0.05 mg S-OMC in 1.0 mL DMF) was drop-casted onto the surface of the GC electrode and dried to obtain an S-OMC/GC modified electrode. A fresh electrode was prepared for each individual measurement. The electrolyte was bubbled with N_2 to remove O_2 before the experiments.

3. Results and discussion

3.1. S-OMC synthesis

Iron was selected as the catalyst for the polymerization of OMC precursors based on literature reports [34,35]. Impregnation of $Fe(NO_3)_3{\cdot}9H_2O$ (0.382 g, 0.945 mmol) on SBA-15 type mesoporous silica nanoparticles (MSN) (1.00 g) followed by calcination led to a small decrease in the surface area of the material (Table 1). SEM imaging of the composite showed no evidence of free iron oxide nanoparticles. However, EDS analysis confirmed the presence of the metal at 1.9 atom% (Table 1, Fig. S1) suggesting it was located inside the mesopores. This result was consistent with a ca. 10% decrease in the pore volume of the material. Impregnation of the Fe-MSN composite with thiophenol followed by carbonization at 600 °C produced a black material (Fig. 1A, left). In contrast, impregnation of iron-free MSN with thiophenol and carbonization at 600 °C led to a gray material, suggesting low carbonization efficiency in absence of the metal (Fig. 1A, right). EDS analysis of the carbonized thiophenol-Fe-MSN composite revealed a homogeneous distribution of C (ca. 50 atom%) and S (ca. 1 atom%) over different areas of the material (Table S1).

Dissolution of the silica template from the composite in aqueous NaOH yielded a S-OMC material with well-defined mesopore structure evidenced by TEM, indicating successful replication of the cylindrical channels of the MSN template (Scheme 1, Fig. 1B). Low angle powder XRD further confirmed the structural relation to the parent MSN showing a sharp reflection at 0.6 2θ degrees associated to the (100) plane of the 2D hexagonal structure (Fig. 1D). Nitrogen sorption analysis of the S-OMC indicated a type IV isotherm (Fig. 1E) characteristic of a mesoporous material with narrow pore width distribution [36] centered at 4.8 nm. Interestingly, the surface area of S-OMC was significantly larger (ca. 150%) than the parent MSN (Table 1), likely due to the lower density of the carbon material. Carbonization at higher temperature (900 °C) led to a drop in surface

Table 1
Textural properties and chemical composition of the materials.

	SA_{BET}[a] ($m^2\ g^{-1}$)	V_{BJH}[b] ($cm^3\ g^{-1}$)	w_{BJH}[c] (nm)	C[d] (at%)	O[d] (at%)	Si[d] (at%)	S[d] (at%)	Fe[d] (at%)
MSN	400	0.97	7.4	–	67.0 ± 1.5	33.0 ± 1.5	–	–
Fe-MSN	385	0.87	7.3	–	61.0 ± 6.5	37.1 ± 6.3	–	1.9 ± 0.3
$S\text{-}OMC_{600}$	596	0.82	4.8	79.8 ± 2.0	15.9 ± 1.8	2.4 ± 0.9	1.5 ± 0.7	0.5 ± 0.1
$S\text{-}OMC_{900}$	388	0.39	3.7	67.2 ± 1.3	27.1 ± 1.3	3.8 ± 0.1	0.5 ± 0.1	1.5 ± 0.1

[a] Surface area calculated by Brunauer–Emmett–Teller method.
[b] Pore volume calculated by Barret–Joyner–Halenda method.
[c] Average pore width calculated by Barret–Joyner–Halenda method.
[d] Obtained from energy dispersive x-ray spectroscopy.

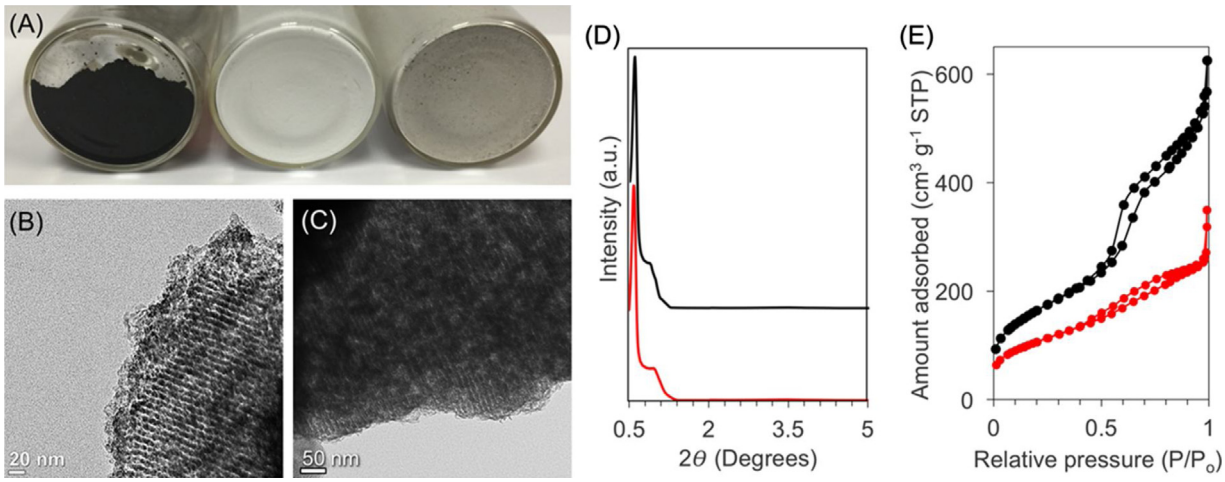

Fig. 1. (A) Carbonized thiophenol-MSN composites with (left) and without (right) iron, and original MSN (middle) for comparison: the gray color of the material without iron suggests incomplete carbonization as opposed to the black carbonized iron-containing material. TEM images of (B) S-OMC$_{600}$ and (C) S-OMC$_{900}$, (D) small-angle X-ray diffraction patterns and (E) N_2 sorption isotherms of S-OMC$_{600}$ (black traces) and S-OMC$_{900}$ (red traces). (For interpretation of the references to colour in this figure legend, the reader is referred to the web version of this article.)

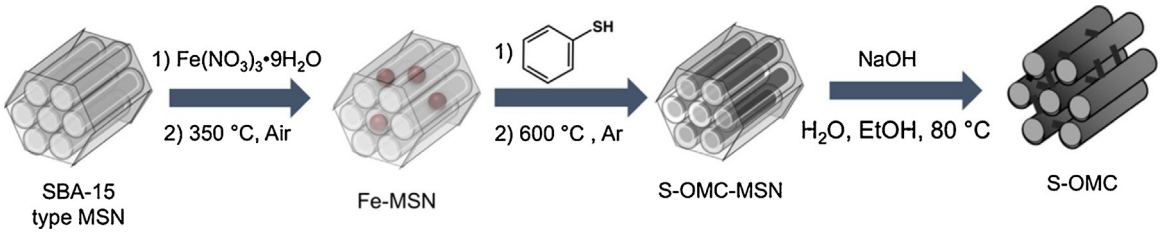

Scheme 1. Steps of S-OMC synthesis.

area, pore volume, and pore width. Subtraction of the pore width from the mesopore unit cell parameter a_0 ($a_0 = (2/\sqrt{3})d_{100}$) revealed that the higher carbonization temperature produced thicker pore walls (11.4 nm at 600 °C versus 13.5 nm at 900 °C). This result indicated that the structure of the material contracted upon thermal treatment, likely due to cross-linking of poly(phenylene sulfide) via formation of S-heterocycles [37]. Increasing the amount of iron in the synthesis also led to smaller surface areas, pore volumes, and pore widths (Table S2).

The wide angle XRD pattern of the S-OMC carbonized at 600 °C (S-OMC$_{600}$) revealed two broad reflections at 23.5 and 44.1 2θ degrees that were indexed as the d_{002} and d_{101} interlayer spacings of carbon planes (Fig. S2A). Both peaks were slightly shifted (26.1 and 42.8) and better defined in the S-OMC carbonized at 900 °C (S-OMC$_{900}$) indicating decreasing d-spacings and an increasing degree of graphitization with carbonization temperature. The d_{002} interlayer spacing of S-OMC$_{900}$ (0.341 nm) was between typical values for turbostratic (0.344 nm) and graphitic carbon (0.335 nm) [38,39]. Reflections attributable to iron oxides were only observed at higher iron loadings, and they appeared to be related to magnetite (Fig. S3) [40]. In fact, all the S-OMCs were attracted to magnets.

Raman spectroscopy of S-OMC$_{600}$ and S-OMC$_{900}$ showed the characteristic D (1300 cm^{-1}) and G (1590 cm^{-1}) bands of sp^2 carbon layers (Fig. S2B) [41]. Because both materials had I_D/I_G ratios larger than 1, the polycyclic aromatic layers must be largely disordered. S-OMC$_{900}$ had a smaller I_D/I_G ratio (1.36) than S-OMC$_{600}$ (1.63), suggesting increasing order (i.e. graphitic character) with carbonization temperature. This result is consistent with the XRD data. Increasing the amount of iron in S-OMC$_{600}$ material also led to lower I_D/I_G ratios (i.e. improved graphitic character, Fig. S3B,C) further confirming that iron promoted carbon graphitization. While XRD and Raman data indicated a more graphitic character of S-OMC$_{900}$ than S-OMC$_{600}$, the S content was significantly lower in the former.

3.2. Electrochemical properties of S-OMC

To study the electrochemical behavior of S-OMC, the materials were suspended in DMF, drop-casted onto clean glassy carbon (GC) electrodes, and dried. The investigation of the modified electrode/electrolyte interface was carried out by cyclic voltammetry (CV) of $[Fe(CN)_6]^{3-/4-}$ (10.0 mmol L^{-1}) from −0.5 to 1.0 V with KCl electrolyte (0.100 mol L^{-1}) at a 100 mV s^{-1} scan rate (Fig. 2). The $[Fe(CN)_6]^{3-/4-}$ redox cycle gave faster electron transfer rates and higher peak currents on the S-OMC$_{900}$ ($\Delta E = 116$ mV, 132 μA/−133 μA) than the S-OMC$_{600}$ ($\Delta E = 144$ mV, 107 μA/−114 μA) modified GC electrodes. These differences indicate that in spite of its smaller surface area S-OMC$_{900}$ is more electroactive than S-OMC$_{600}$, likely due to the higher conductivity resulting from the increased graphitic character and smaller d-spacing of the former.

3.3. Application of S-OMC/GC as chloramphenicol sensors

As a proof-of-concept, the two S-OMC/GC electrodes were used to examine the electrochemical behavior of chloramphenicol (CAP) solutions. The cyclic voltammograms of CAP (3.00 mmol L^{-1}) using the S-OMC/GC as working electrodes in 0.100 mol L^{-1} H_2SO_4 at a 100 mV s^{-1} scan rate presented well-defined cathodic and anodic peaks (Fig. 3). The peak currents obtained with the S-OMC modified

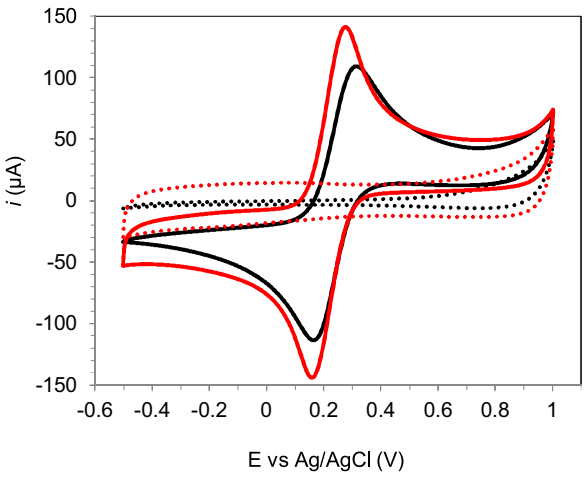

Fig. 2. Cyclic voltammogram in absence (····) and presence (–) of 10.0 mmol L^{-1} $[Fe(CN)_6]^{3-/4-}$ in 0.100 mol L^{-1} KCl using GC, S-OMC_{600}/GC (black traces) or S-OMC_{900}/GC (red traces) as working electrode. (For interpretation of the references to colour in this figure legend, the reader is referred to the web version of this article.)

electrodes were higher and appeared at lower potentials than with the bare GC electrode. The main cathodic peak appeared at a more negative potential for S-OMC_{600}/GC (−343 mV) than S-OMC_{900}/GC (−270 mV), and was attributed to the irreversible reduction of the nitro group to an amine via an hydroxylamine intermediate (Eqs. (1) and (2)) [42–46]. The 73 mV shift and fourfold peak current enhancement observed using S-OMC_{900}/GC compared to S-OMC_{600}/GC indicated the former was a more efficient electrocatalyst for the reduction of the nitro group in CAP than the latter. This behavior is consistent with the results obtained from the cyclic voltammetry of $Fe(CN)_6^{-4/-3}$, and can therefore be attributed to the increased graphitic character of S-OMC_{900}. The voltammograms of the reaction using S-OMC_{600}/GC presented two additional well-defined redox peaks (E_{PC} = 307 mV; E_{PA} = 340 mV). These peaks are associated with excess hydroxylamine intermediate that can be reversibly oxidized to a nitroso group (Eq. (3)) [47,48]. Interestingly, these peaks were significantly less evident when using S-OMC_{900}/GC, suggesting lower adsorption of the hydroxylamine intermediate onto S-OMC_{900} than S-OMC_{600}.

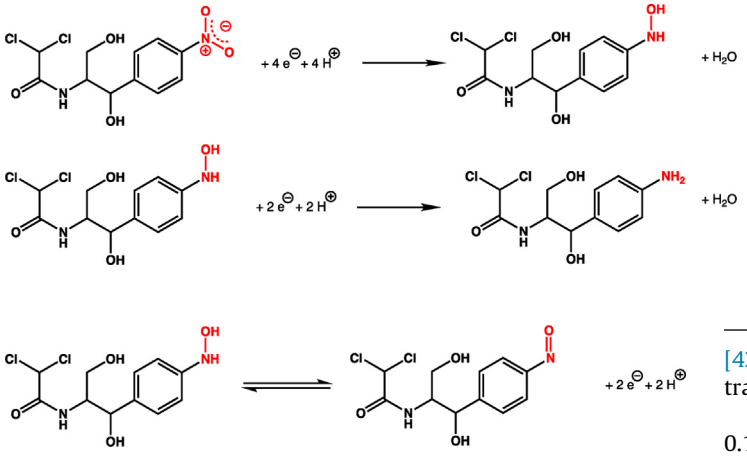

The effect of scan rate on the cathodic peak current (−270 mV) was investigated to obtain more insights into the mechanism of the electrochemical reduction of the nitro group in CAP. The CV were acquired from 0 to −600 mV in H_2SO_4 0.100 mol L^{-1} using S-OMC_{900}/GC as working electrode with scan rates varying from 50 to 400 mV s^{-1} (Fig. S4). A linear correlation (R^2 = 0.999) between the cathodic peak current (I_P) and the scan rate (ν) was found. This suggested that the exponent in the equation $I_P = A\nu^x$ should be close to 1, indicating that the irreversible transformation should be an adsorption-controlled process [49]. To verify the value of x, the correlation between the logarithm of the peak current and the logarithm of the scan rate was calculated, obtaining a linear behavior (R^2 = 0.999) with a slope (x) of 1.3. The slope was close to the ideal value of 1.0, as expected for adsorption-controlled reactions [50]. This behavior indicated that the high surface area of the S-OMC materials was critical to their electrochemical performance. Furthermore, the open mesoporous structure and large pore volume of S-OMC should be key to maximize the accessibility of the analyte to the electrochemically active surface, and allow loading large amounts of the target molecules (on the order of mmol g^{-1}) [2,51]. This result suggested that including a pre-concentration step should increase the capacity of detecting CAP with S-OMC/GC. To explore this possibility, a linear sweep voltammetry (LSV) of CAP (3.0 mmol L^{-1} in 0.100 mmol L^{-1} H_2SO_4) was performed using S-OMC_{900}/GC as the working electrode with open circuit pre-accumulation steps of variable times. The results indicated that the peak current increased with pre-accumulation time in the range of 0–360 s, but no further increase was observed at longer times (Fig. S5). Therefore, a 360 s pre-accumulation step was applied to all of the following experiments.

The effect of acidity on the behavior of the electrochemical reduction of CAP was investigated using phosphate buffered saline (PBS) solutions at pH varying from 1.9 to 10.4 and a 100 mV s^{-1} scan rate (Fig. S6). The peak potential was strongly pH dependent and shifted linearly to negative values with increasing pH (R^2 = 0.997, ca. −47 mV per pH unit). This result is explained by the fact that the electrochemical reduction of the nitro group requires 4 H^+ per molecule to transform into hydroxylamine (Eq. (1)) and two additional H^+ per molecule for the full conversion to amine (Eq. (2)). Since increasing pH implies a decrease in the concentration of available protons, higher pH values shift the equilibrium of the reduction to the reactants, which based on Nernst equation drives the reduction potential to increasingly negative values. In addition, it has been reported that the rate limiting step of the electrochemical reduction of nitroaromatic compounds involves protonation of the nitro group to form a more readily reducible intermediate [42,52–54]. Therefore increasing pH implies lower proton concentration, which directly decreases the rate of protonation.

Because of the lower potential needed in acid electrolytes, a 0.100 mol L^{-1} H_2SO_4 solution was used to prepare a calibration curve for the quantification of the drug (Fig. 4). The curve was constructed using LSV in the range 0 to −0.5 mV at a 100 mV s^{-1} scan rate with S-OMC_{900}/GC as the working electrode. The reduction peak current (−270 mV) increased linearly (R^2 = 0.992) with chloramphenicol concentration (0.1–1.0 μmol L^{-1}) with a sensitivity of 11.7 A L mol^{-1}. It must be noted that higher concentrations of CAP gave a lower sensitivity. The limits of detection and quantification were calculated as 0.013 μmol L^{-1} and 0.043 μmol L^{-1} respectively

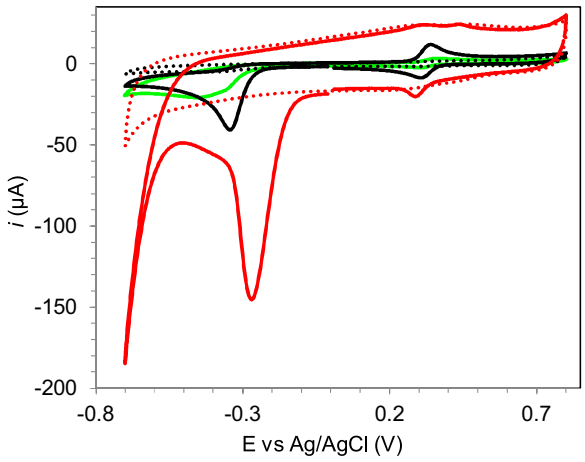

Fig. 3. Cyclic voltammograms in absence (····) and presence (--) of 3.0 mmol L^{-1} chloramphenicol in 0.100 mol L^{-1} H_2SO_4 electrolyte, using GC (green trace), S-OMC_{600}/GC (black trace) or S-OMC_{900}/GC (red trace) as the working electrode. (For interpretation of the references to colour in this figure legend, the reader is referred to the web version of this article.)

(LOD = 3SD/S, LOQ = 10SD/S, where SD is the standard deviation of 10 blank measurements (0.050×10^{-8} μA) and S is the sensitivity). The obtained values were comparable or better than other electrodes reported in the literature (Table S2), and highly repeatable, with a 2.3% relative standard deviation (RSD) for ten consecutive measurements (Fig. S7a). The reproducibility of preparation of the S-OMC modified GC electrodes was estimated by comparing the performances of three freshly produced electrodes (Fig. S7b). The low RSD (1.8%) obtained for the peak reduction current measurements demonstrated a highly reproducible manufacturing method.

To investigate the selectivity of the sensor, thiamphenicol (TAP) and florfenicol (FLF), two allowed antibiotics with structures similar to CAP (Fig. 5A–D), were analyzed as controls. Because ampicillin (AMP) is usually administered in association with CAP, its potential interference with the detection of the latter was also evaluated. Cyclic voltammetry experiments in H_2SO_4 0.100 mol L^{-1} at 100 mV s^{-1} scan rate of TAP, FLF, AMP (1.0 mmol L^{-1} each) and combinations thereof revealed no peak in the range 0 to −600 mV, indicating none of the functionalities in these antibiotics was reducible in the same regime as the nitro group in CAP (Fig. 5G). Addition of CAP (1.0 mmol L^{-1}) to a mixture containing all of these antibiotics led to a dramatic increase in current, demonstrating that the method is selective with respect to these allowed substances.

To further evaluate if the signal is specific to the reduction of the nitro group, the method was applied to the analysis of two pesticide molecules -fenitrothion and parathion methyl- that contain this functionality (Fig. S8). The CV was carried out in H_2SO_4 0.100 mol L^{-1} at a 100 mV s^{-1} scan rate. An increase in the reduction peak of CAP was observed upon addition of each substance (0.5 mmol L^{-1} each), further suggesting the signal corresponds to the reduction of the nitro moiety. While these substances are potential interferents to the detection of chloramphenicol, this method can be useful as a quick and simple screen for the presence of any of these dangerous substances and serve as a criterion to decide if a sample merits a more thorough analysis.

To determine whether the S-OMC_{900}/GC electrode could be used to quantify CAP in milk, a sample was prepared by dissolving commercial powdered milk in aqueous H_2SO_4 (0.100 g in 10 mL, 0.100 mol L^{-1}) and analyzed directly, without any further

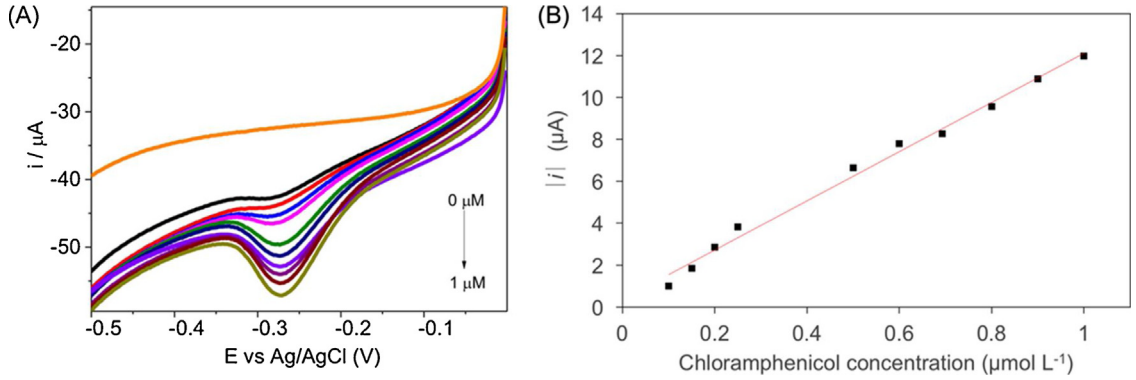

Fig. 4. (A) LSV of increasing concentrations of chloramphenicol (0.10, 0.15, 0.20, 0.25, 0.50, 0.60, 0.80, 0.90, 1.0 μmol L^{-1}) using S-OMC_{900}/GC electrode in H_2SO_4 0.100 mol L^{-1}, acquired from 0 to −0.5 V at a scan rate 100 mV s^{-1}. (B) Plot of reduction peak current intensity (−270 mV) versus chloramphenicol concentration.

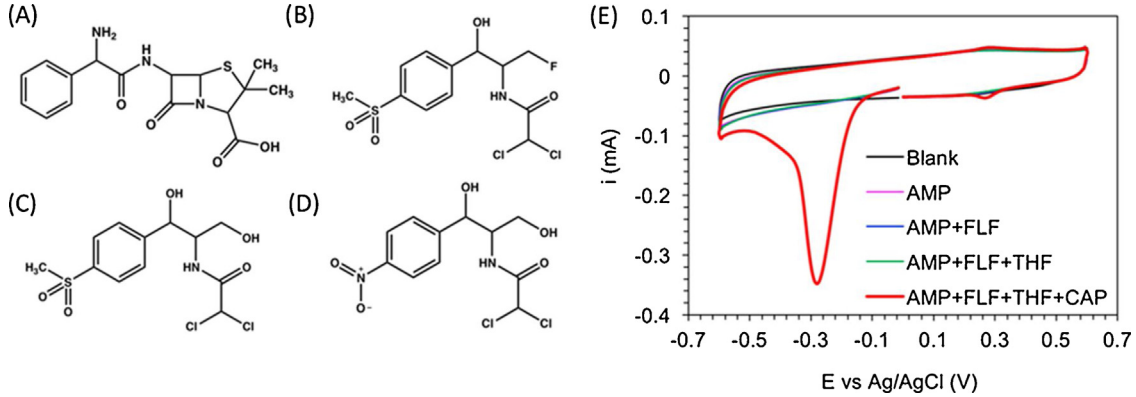

Fig. 5. Chemical structures of (A) ampicillin (AMP), (B) florfenicol (FLF), (C) thiamphenicol (THF), and (D) CAP. (E) Cyclic voltammetry in absence and presence of AMP, FLF, THF and CAP (1.0 mmol L^{-1} each) in H_2SO_4 0.1 mol L^{-1} using S-OMC_{900}/GC as working electrode.

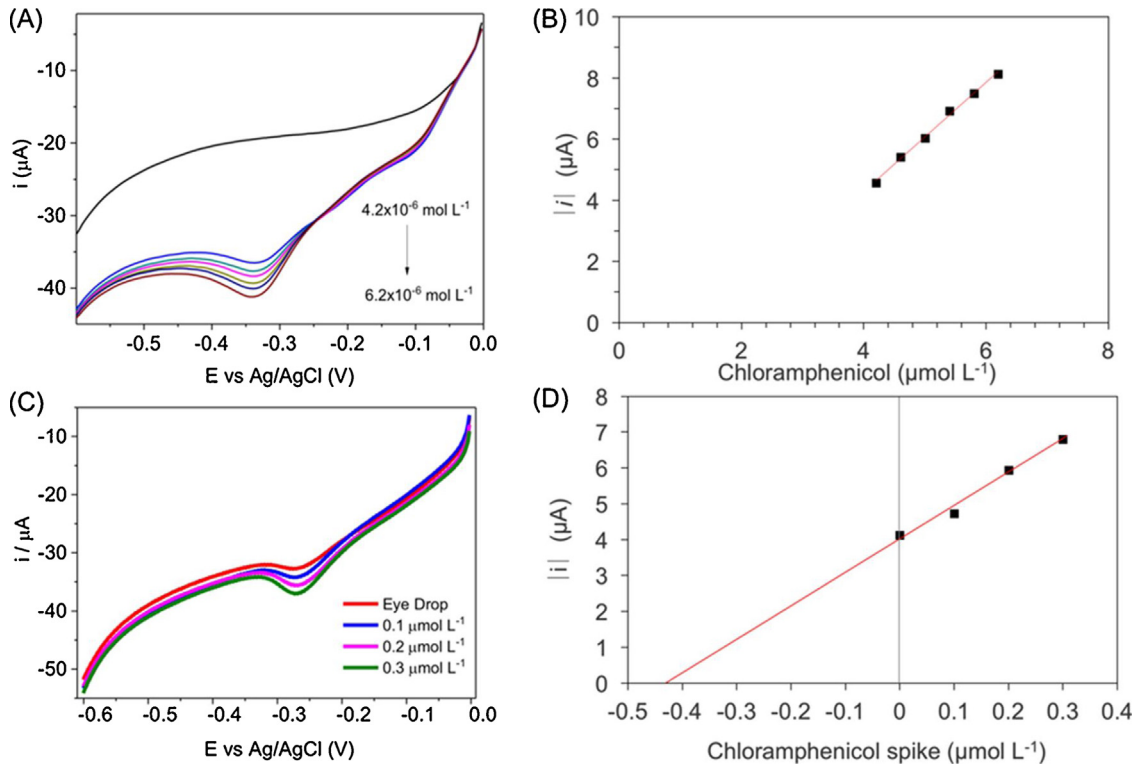

Fig. 6. (A) LSV of milk samples dissolved in H_2SO_4 0.100 mol L^{-1} with increasing concentrations of CAP (0, 4.2, 4.6, 5.0, 5.4 and 6.2 μmol L^{-1}) using S-OMC_{900}/GC electrode acquired from 0 to −0.5 V at a scan rate 100 mV, and (B) the corresponding plot of reduction peak current intensity (−340 mV) versus CAP concentration. Quantification of CAP in commercial eye drops via standard addition: (C) LSV plots (0 to −0.5 V, scan rate 100 mV s^{-1}, S-OMC_{900}/GC electrode, diluted in H_2SO_4 0.100 mol L^{-1}), and (D) the corresponding plot of reduction peak current intensity (−270 mV) versus CAP concentration.

processing. The LSV from 0 to −0.6 V (100 mV s^{-1} scan rate) of the reconstituted milk using the S-OMC_{900}/GC electrode showed no interfering peaks at the detection potential. Upon addition of CAP in the 4.20–6.20 μmol L^{-1} concentration range, a linear analytical response (R^2 = 0.999, Fig. 6A, B) was obtained with good sensitivity (1.78 A L mol^{-1}) just one order of magnitude smaller than the sensitivity in 0.1 mmol L^{-1} H_2SO_4, with a 0.12 μmol L^{-1} LOD and a 0.39 μmol L^{-1} LOQ (SD = 0.070 μA). These results indicate partial interference of the matrix, possibly due to adsorption of milk proteins on the surface of S-OMC, and limits the application of this analysis to ppm concentrations of nitro-aromatics in milk.

Finally, the method was applied to the analysis of a sample of commercial eye drops with a reported concentration of CAP of 4.0 mg mL^{-1} or 12×10^{-3} mol L^{-1} based on the label. The sample was diluted 100-fold with deionized water (10.0 μL to 1.00 mL), and a 64.6 μL aliquot of this dilution was mixed with H_2SO_4 0.100 mol L^{-1} to a final volume of 20.0 mL (total dilution factor: 3.10×10^4). The mixture was then spiked with CAP to obtain solutions with increments of 0.100, 0.200 and 0.300 μmol L^{-1}. The S-OMC_{900}/GC was then used as the working electrode to perform an LSV from 0 to −0.6 V at a 100 mV s^{-1} scan rate (Fig. 6C, D). The plot of concentration versus the peak current increased linearly (R^2 = 0.985) following the relationship i = 9.23*C + 4.01 (i = current in μA and C = concentration in μmol L^{-1}, Fig. 6). By extrapolation to i = 0 the concentration of CAP in the diluted sample was calculated as 0.434 μmol L^{-1}, which multiplied by the dilution factor gave 1.35×10^4 μmol L^{-1} or 4.35 mg mL^{-1}. This implies a difference of 8.7% with respect to the concentration indicated in the label.

4. Conclusions

Thiophenol was effectively used as a new carbon source for producing S-doped OMC with SBA-15 type mesoporous silica nanoparticles as a hard template. The process required iron to facilitate carbon formation, and the graphitic character increased with the amount of iron employed in the synthesis. The carbonization temperature controlled two properties relevant to the electrochemical performance of the materials: increasing carbonization temperatures resulted in increasing graphitic character but decreasing surface area of the carbons. The S-OMC were drop-casted on glassy carbon electrodes, and tested in the CV of the redox probe $[Fe(CN)_6]^{3-/4-}$. The S-OMC modified GC electrodes presented small charge transfer resistance and high peak currents. The lower potential and higher currents obtained with S-OMC_{900}/GC than S-OMC_{600}/GC suggested that the higher graphitic character of the former was more relevant to the electrochemical performance than the higher surface area of the latter. Further testing of the modified S-OMC/GC electrodes in voltammetric analysis of CAP revealed dramatic differences between both electrodes, especially in the reduction of the nitro group, which had significantly lower potential and higher currents with S-OMC_{900}/GC. The high response of the modified electrode to the reduction of the nitro group allowed using it for the selective detection and quantification of the forbidden CAP in presence of the allowed antibiotics florfenicol and thiamphenicol. The specificity for the nitro reduction was confirmed by evaluating the response to two nitro-aromatic pesticides (fenitrothion and parathion methyl) suggesting this method could be useful for the simple and quick detection of dangerous chemicals in the ppm range. The applicability of the method was successfully tested by the direct analysis of commercial powdered milk and eye drops with no other preparation step than mere dilution with 0.100 mmol L^{-1} H_2SO_4. Further improvements of the S-OMC materials such as controlling the amount of dopant and optimizing the balance between surface area and graphitic character should lead to modified electrodes with higher sensitivity and lower detection and quantification limits.

Acknowledgments

The authors thank CAPES and CNPq for financial support, INCT/INOMAT – National Institute of Science, Technology and Innovation in Complex Functional Materials (CNPq-MCTI/Fapesp) for TEM images. U.C., J.S.M. and I.I.S. acknowledge funding support from the U.S. Department of Energy, Office of Basic Energy Sciences, Division of Chemical Sciences, Geosciences, and Biosciences through the Ames Laboratory. The Ames Laboratory is operated for the U.S. Department of Energy by Iowa State University under Contract No. DE-AC02-07CH11358.

Appendix A. Supplementary data

Supplementary data associated with this article can be found, in the online version, at https://doi.org/10.1016/j.snb.2017.10.164.

References

[1] J.C. Ndamanisha, L.-p. Guo, Anal. Chim. Acta 747 (2012) 19–28.
[2] A. Walcarius, Trends Anal. Chem. 38 (2012) 79–97.
[3] T.-W. Kim, P.-W. Chung, I.I. Slowing, M. Tsunoda, E.S. Yeung, V.S.-Y. Lin, Nano Lett. 8 (2008) 3724–3727.
[4] Y. Zhou, L. Tang, G. Zeng, J. Chen, Y. Cai, Y. Zhang, G. Yang, Y. Liu, C. Zhang, W. Tang, Biosens. Bioelectron. 61 (2014) 519–525.
[5] F. Li, J. Song, C. Shan, D. Gao, X. Xu, L. Niu, Biosens. Bioelectron. 25 (2010) 1408–1413.
[6] J.B. Raoof, F. Chekin, R. Ojani, S. Barari, M. Anbia, S. Mandegarzad, Anglais 16 (2012) 8.
[7] Y. Zhang, X. Bo, A. Nsabimana, C. Luhana, G. Wang, H. Wang, M. Li, L. Guo, Biosens. Bioelectron. 53 (2014) 7.
[8] R. Ryoo, S.H. Joo, M. Kruk, M. Jaroniec, Adv. Mater. 13 (2001) 677–681.
[9] H. Chang, S.H. Joo, C. Pak, J. Mater. Chem. 17 (2007) 3078–3088.
[10] C.H. Kim, D.-K. Lee, T.J. Pinnavaia, Langmuir 20 (2004) 5157–5159.
[11] T.-W. Kim, I.-S. Park, R. Ryoo, Angew. Chem. 115 (2003) 4511–4515.
[12] Y. Xia, R. Mokaya, Adv. Mater. 16 (2004) 1553–1558.
[13] W. Gao, Y. Wan, Y. Dou, D. Zhao, Adv. Energy Mater. 1 (2011) 115–123.
[14] Z. Wu, Y. Yang, D. Gu, Y. Zhai, D. Feng, Q. Li, B. Tu, P.A. Webley, D.Y. Zhao, Top. Catal. 52 (2009) 12–26.
[15] R. Liu, D. Wu, X. Feng, K. Müllen, Angew. Chem. 122 (2010) 5.
[16] X. Liang, Z. Wen, Y. Liu, H. Zhang, L. Huang, J. Jin, J. Power Source 196 (2011) 3655–3658.
[17] H. Wang, C. Zhang, Z. Chen, H.K. Liu, Z. Guo, Carbon 81 (2015) 782–787.
[18] S.-R. Chen, Y.-P. Zhai, G.-L. Xu, Y.-X. Jiang, D.-Y. Zhao, J.-T. Li, L. Huang, S.-G. Sun, Electrochim. Acta 56 (2011) 9549–9555.
[19] H.I. Lee, S.H. Joo, J.H. Kim, D.J. You, J.M. Kim, J.-N. Park, H. Chang, C. Pak, J. Mater. Chem. 19 (2009) 5934–5939.
[20] K. Kwon, S.-A. Jin, C. Pak, H. Chang, S.H. Joo, H.I. Lee, J.H. Kim, J.M. Kim, Catal. Today 164 (2011) 186–189.
[21] H. Wang, X. Bo, Y. Zhang, L. Guo, Electrochim. Acta 108 (2013) 404–411.
[22] A.P. Terzyk, G. Rychlicki, Colloid Surf. A: Physicochem. Eng. Aspects 163 (2000) 135–150.
[23] A.P. Terzyk, Colloid Surf. A: Physicochem. Eng. Aspects 177 (2001) 23–45.
[24] M. Seredych, K. László, T.J. Bandosz, ChemCatChem 7 (2015) 2924–2931.
[25] R. Yang, Y. Sun, Z. Yang, J. Wu, Facile synthesis and electrocatalytic activity of sulfur doped carbon for oxygen reduction, in: Meeting Abstracts, The Electrochemical Society, 2015, 736–736.
[26] M. Seredych, T.J. Bandosz, Carbon 49 (2011) 1216–1224.
[27] M. Seredych, M. Khine, T.J. Bandosz, ChemSusChem 4 (2011) 139–147.
[28] T.L. Fodey, S.E. George, I.M. Traynor, P. Delahaut, D.G. Kennedy, C.T. Elliott, S.R.H. Crooks, J. Immunol. Methods 393 (2013) 30–37.
[29] J. Ferguson, A. Baxter, P. Young, G. Kennedy, C. Elliott, S. Weigel, R. Gatermann, H. Ashwin, S. Stead, M. Sharman, Anal. Chim. Acta 529 (2005) 109–113.
[30] F.T. Fraunfelder, G.C. Bagby, D.J. Kelly, Am. J. Ophthalmol. 93 (1982) 356–360.
[31] K. Krasinski, R. Perkin, J.C. Rutledge, Clin. Pediatr. 21 (1982) 571–572.
[32] E. Commission, RASFF Portal, 2017.
[33] K. Kandel, U. Chaudhary, N.C. Nelson, I.I. Slowing, ACS Catal. 5 (2015) 6719–6723.
[34] W. Li, S. Xie, L. Qian, B. Chang, Science 274 (1996) 1701.
[35] S. Li, G.D. Meitzner, E. Iglesia, J. Phys. Chem. B 105 (2001) 5743–5750.
[36] J. Xu, Z. Luan, H. He, W. Zhou, L. Kevan, Chem. Mater. 10 (1998) 3690–3698.
[37] A. Oya, K. Arai, K. Fujita, J. Mater. Sci. 29 (1994) 4477–4480.
[38] G. Bacon, Acta Crystallogr. 4 (1951) 558–561.
[39] U. Rost, R. Muntean, P. Podleschny, G. Marginean, M. Brodmann, V.A. Şerban, Influence of the Graphitisation degree of carbon nano fibres serving as support material for noble metal electro catalysts on the performance of PEM fuel cells, in: Solid State Phenomena, Trans Tech Publ, 2016, pp. 27–32.
[40] X. Dong, H. Chen, W. Zhao, X. Li, J. Shi, Chem. Mater. 19 (2007) 3484–3490.
[41] F. Su, J. Zeng, X. Bao, Y. Yu, J.Y. Lee, X. Zhao, Chem. Mater. 17 (2005) 3960–3967.
[42] A. Morales, P. Richter, M.I. Toral, Analyst 112 (1987) 965–970.
[43] B. Ortiz, C. Saby, G. Champagne, D. Bélanger, J. Electroanal. Chem. 455 (1998) 75–81.
[44] H. Tsutsumi, S. Furumoto, M. Morita, Y. Matsuda, J. Colloid Interface Sci. 171 (1995) 505–511.
[45] M. Feng, D. Long, Y. Fang, Anal. Chim. Acta 363 (1998) 67–73.
[46] D. Guziejewski, S. Skrzypek, A. Łuczak, W. Ciesielski, Collect. Czech. Chem. Commun. 76 (2011) 131–142.
[47] J. Borowiec, R. Wang, L. Zhu, J. Zhang, Electrochim. Acta 99 (2013) 138–144.
[48] H. Zhao, Y. Chen, J. Tian, H. Yu, X. Quan, J. Electrochem. Soc. 159 (2012) 6.
[49] N. Erk, Anal. Biochem. 323 (2003) 48–53.
[50] D. Zheng, J. Ye, L. Zhou, Y. Zhang, C. Yu, J. Electroanal. Chem. 625 (2009) 82–87.
[51] J. Zang, C.X. Guo, F. Hu, L. Yu, C.M. Li, Anal. Chim. Acta 683 (2011) 187–191.
[52] E. Laviron, A. Vallat, R. Meunier-Prest, J. Electroanal. Chem. 379 (1994) 427–435.
[53] E. Laviron, L. Roullier, J. Electroanal. Chem. Interfacial Electrochem. 288 (1990) 165–175.
[54] M. Zanoni, I. Rosa, C. Pesquero, N.R. Stradiotto, J. Braz. Chem. Soc. 8 (1997) 223–227.

Biographies

Dr. Jaqueline R. Maluta obtained her PhD in 2017 at the University of Sao Paulo under the supervision of Dr. Sergio A.S. Machado, and had a research internship at Iowa State University in 2016 under the supervision of Igor I. Slowing.

Dr. Sergio A.S. Machado is a professor at Sao Carlos Institute of Chemistry of the University of Sao Paulo, Brazil, and the coordinator of the Group of Electrochemical Materials and Electroanalytical Methods (GMEME).

Umesh Chaudhary obtained his MSc from Iowa State University studying heterogeneous catalysts under the supervision of Igor I. Slowing.

J. Sebastián Manzano is currently a graduate student working on additive manufacturing of chemically active materials at Iowa State University under the supervision of Igor I. Slowing.

Dr. Lauro T. Kubota is the director of the Chemistry Institute of the University of Campinas, Sao Paulo, and the coordinator of the Laboratory of Electrochemistry, Electroanalytics and Sensor Development (LEEDS).

Dr. Igor I. Slowing is a Senior Scientist at the US Department of Energy Ames National Laboratory and adjunct professor of chemistry at Iowa State University, USA, and his research focuses on developing multifunctional nanostructured materials for catalysis, sensing and adsorption.